Electronic Supplementary Material (ESI) for Materials Chemistry Frontiers.

Supporting Information

An Efficient Star-Shaped Fused-Ring Electron Acceptor with C_{3h}-Symmetric Core via Thieno[3,2-b]thiophene Extending Conjugation Strategy

Weijie Wang, [a,b] Tong Wang, [a,b] Xiaofu Wu,*[a] Hui Tong, [a,b] and Lixiang Wang*[a,b]

[a] *State Key Laboratory of Polymer Physics and Chemistry, Changchun Institute of Applied, Chinese Academy of Sciences, Changchun 130022, P. R. China.*
[b] *University of Science and Technology of China, Hefei 230026, P. R. China.*

*Corresponding author.
E-mail address: wxp@ciac.ac.cn, lixiang@ciac.ac.cn

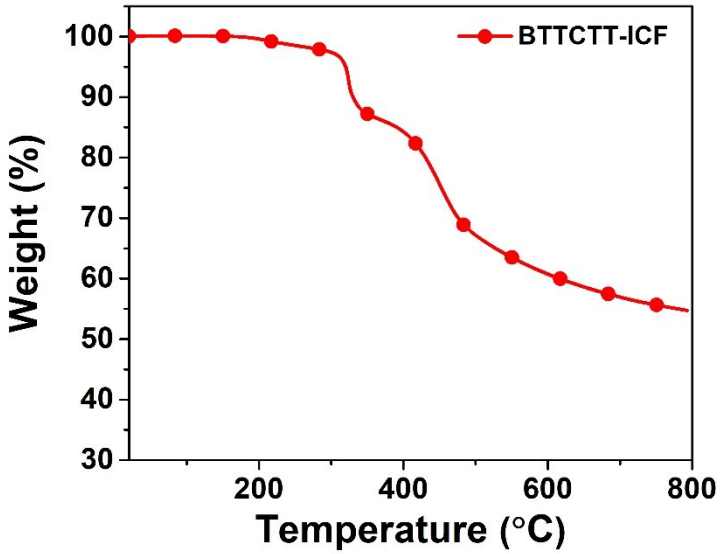

Fig. S1. TGA curves of **BTTCTT-ICF**.

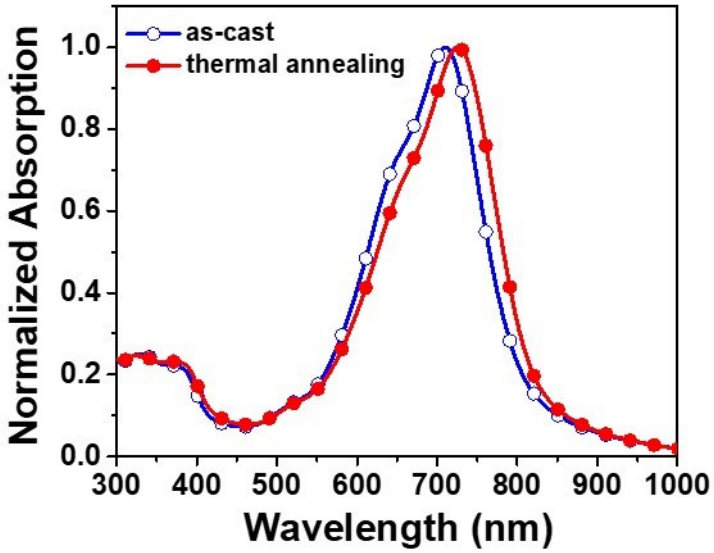

Fig. S2. UV-vis absorption spectra of **BTTCTT-ICF** in thin film before and after annealing at 200 °C.

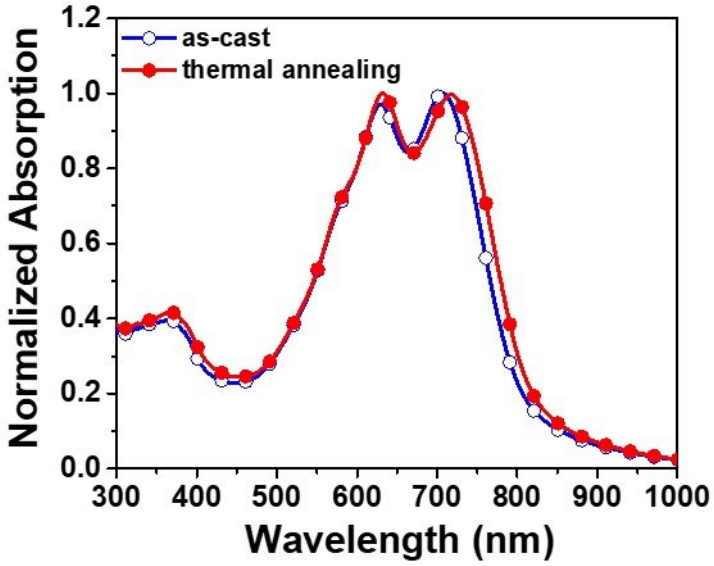

Fig. S3. UV-vis absorption spectra of **PM6**: **BTTCTT-ICF** blend film before and after thermal annealing at 200 °C.

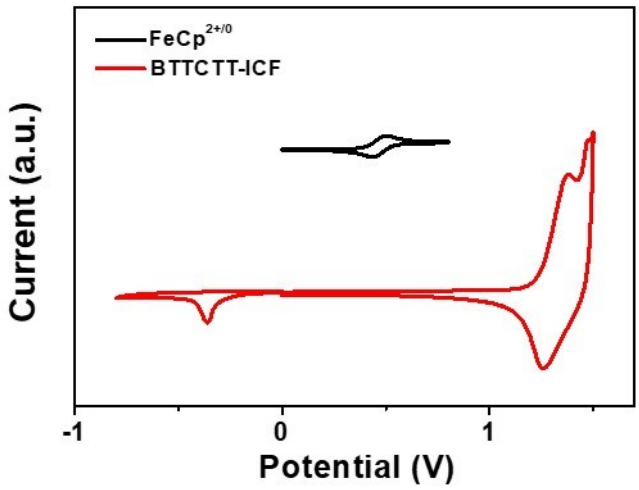

Fig. S4. Cyclic voltammograms of **BTTCTT-ICF** in thin film.

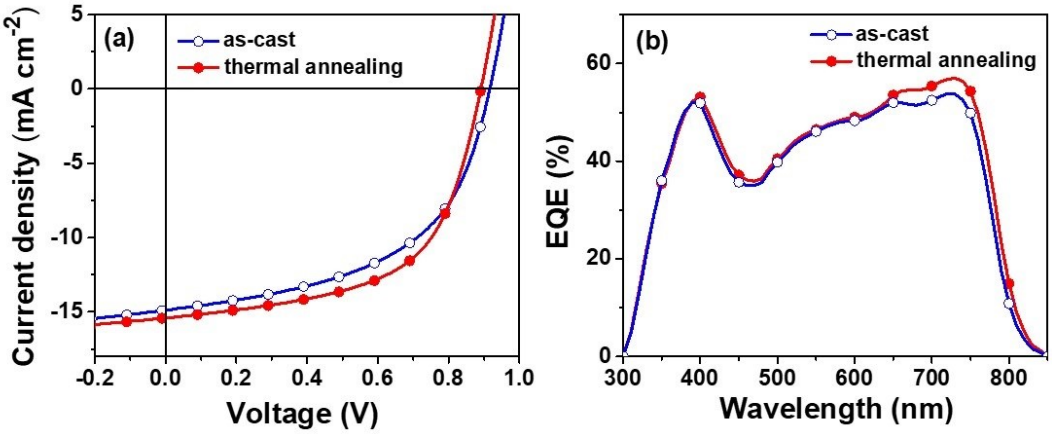

Fig. S5. (a) *J*-*V* characteristics and (b) EQE spectra of the OSCs based on **PM6**: **BTTCTT-ICF** with conventional structures under illumination of an AM 1.5 G at 100 mW cm^{-2}.

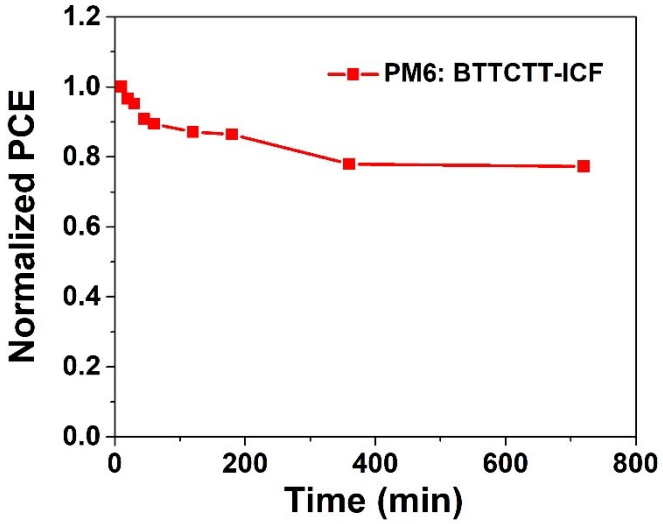

Fig. S6. The normalized PCEs for the devices based on **PM6**: **BTTCTT-ICF** blend films after thermal annealing at 200 °C for different time.

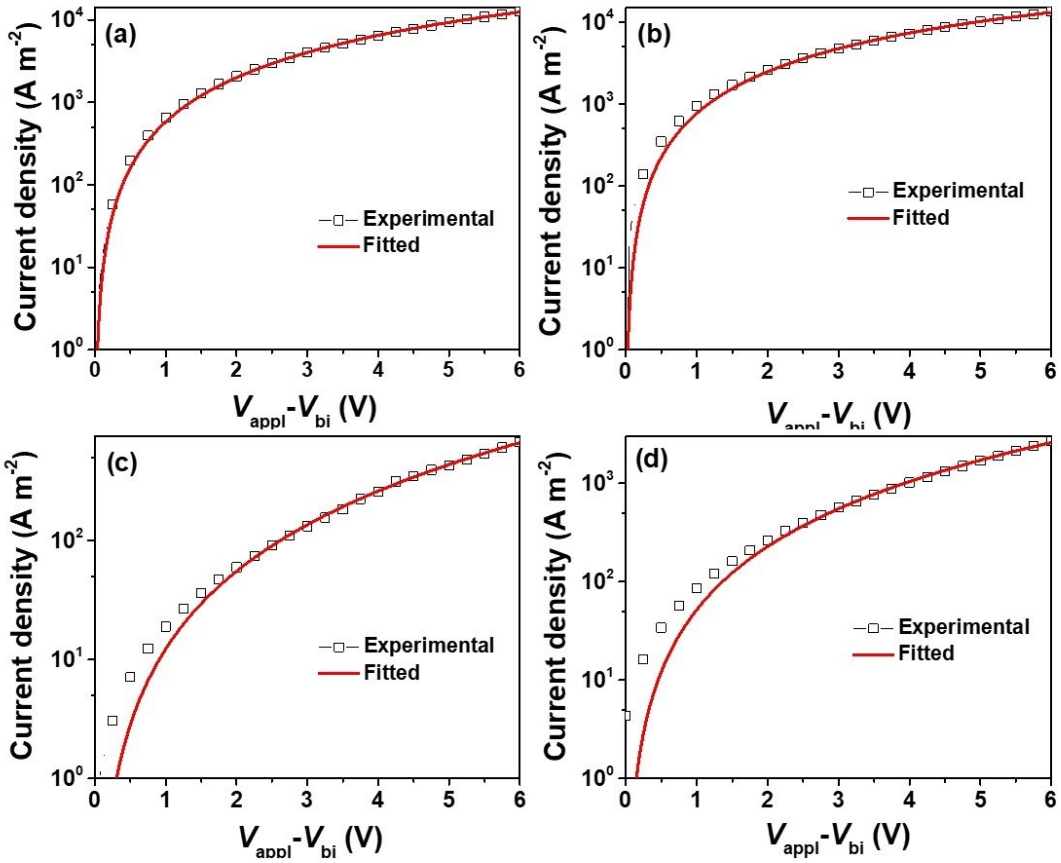

Fig. S7. *J-V* curves and SCLC fittings of hole-only devices for (a) as-cast and (b) thermal annealed **PM6**: **BTTCTT-ICF** blend films; electron-only devices for (c) as-cast and (d) thermal annealed **PM6**: **BTTCTT-ICF** blend films.

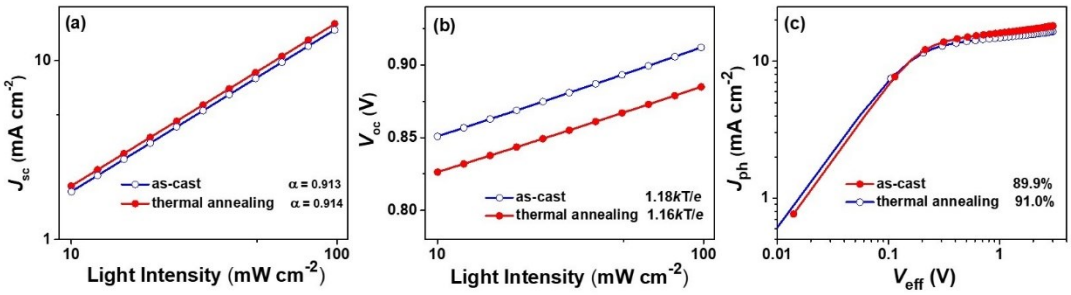

Fig. S8. (a) J_{sc} versus light intensity, (b) V_{oc} versus light intensity and (c) Photocurrent versus effective voltage of OSCs based on **PM6**: **BTTCTT-ICF** with inverted device structure.

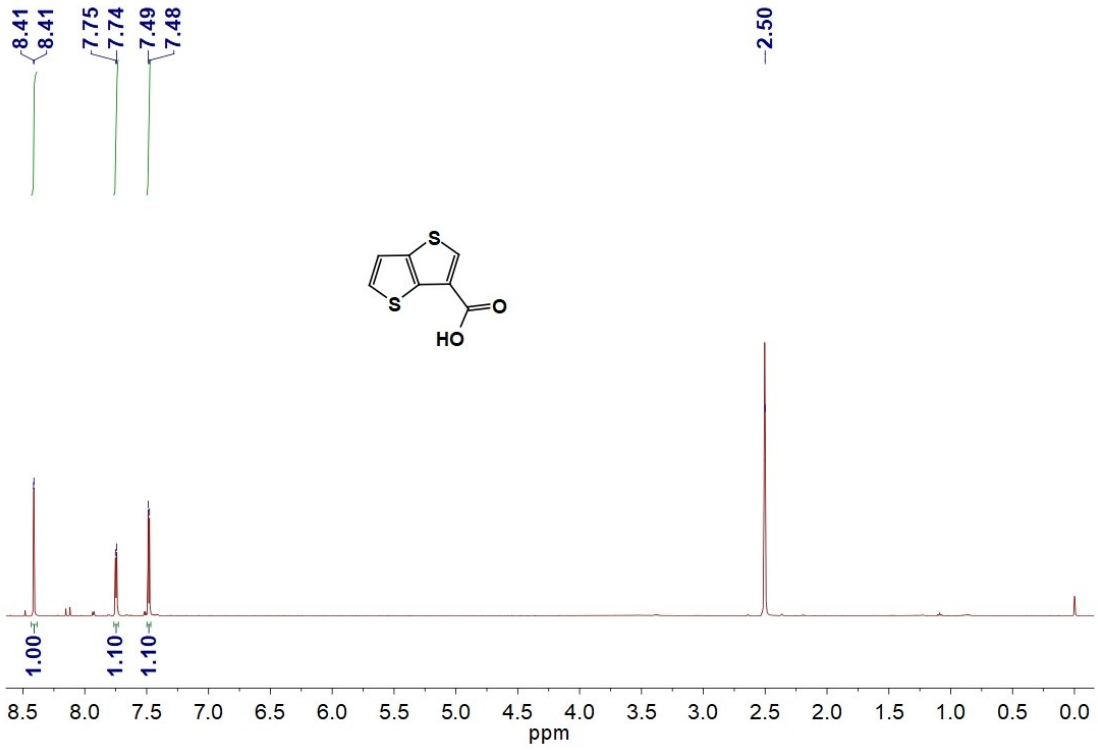

Fig. S9. ^{1}H NMR of compound **2**.

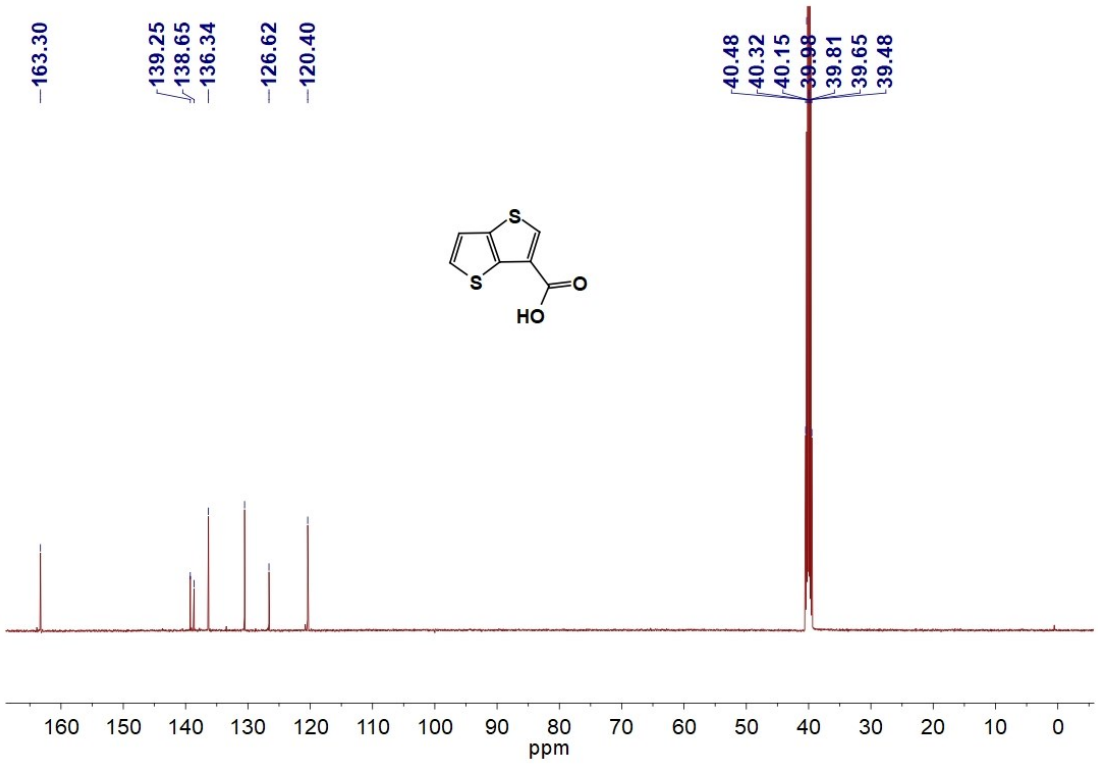

Fig. S10. ^{13}C NMR of compound **2**.

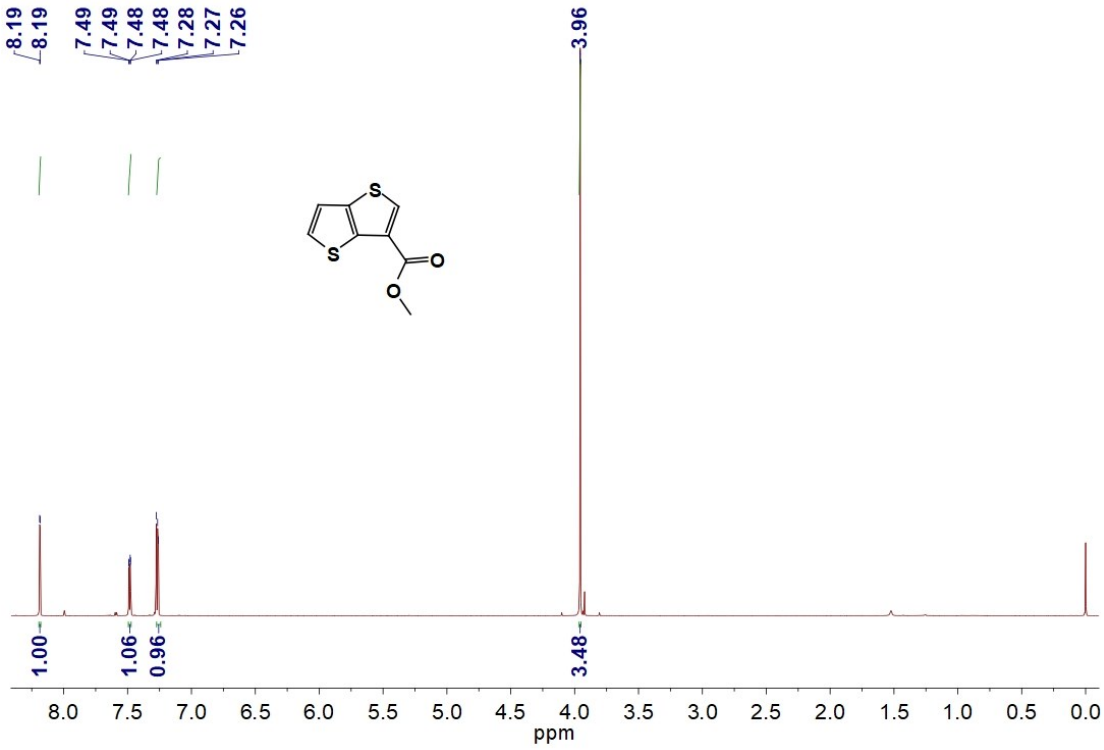

Fig. S11. ^{1}H NMR of compound **3**.

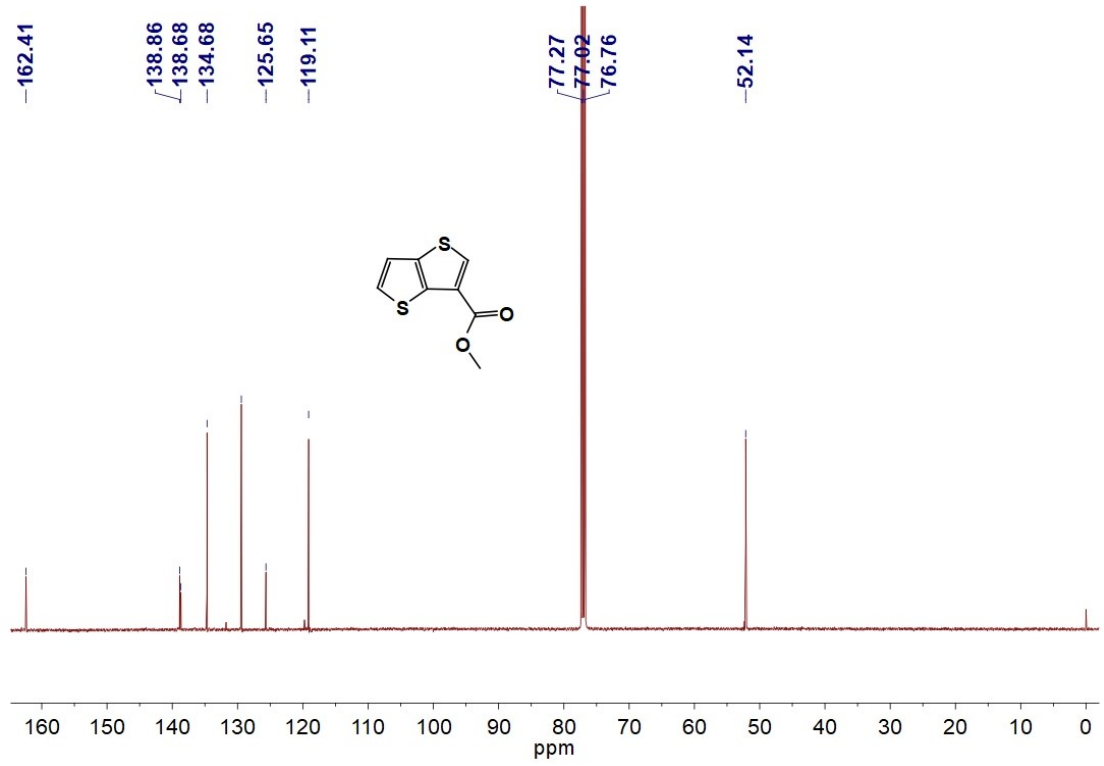

Fig. S12. ^{13}C NMR of compound **3**.

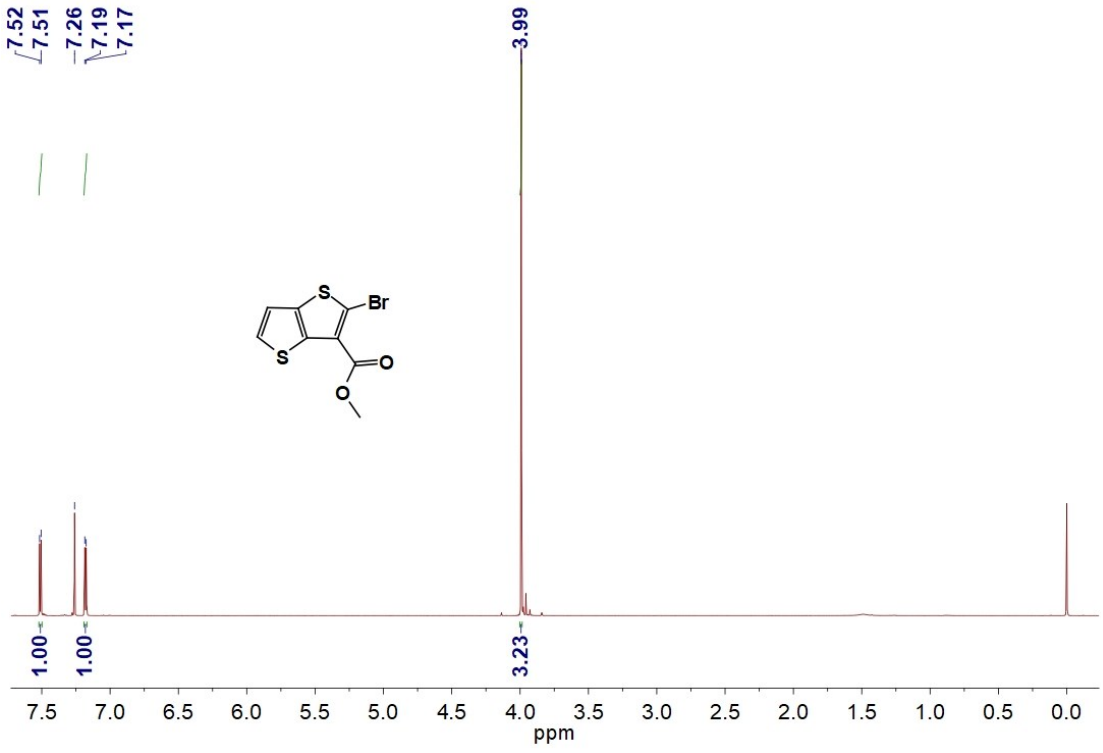

Fig. S13. ^{1}H NMR of compound **4**.

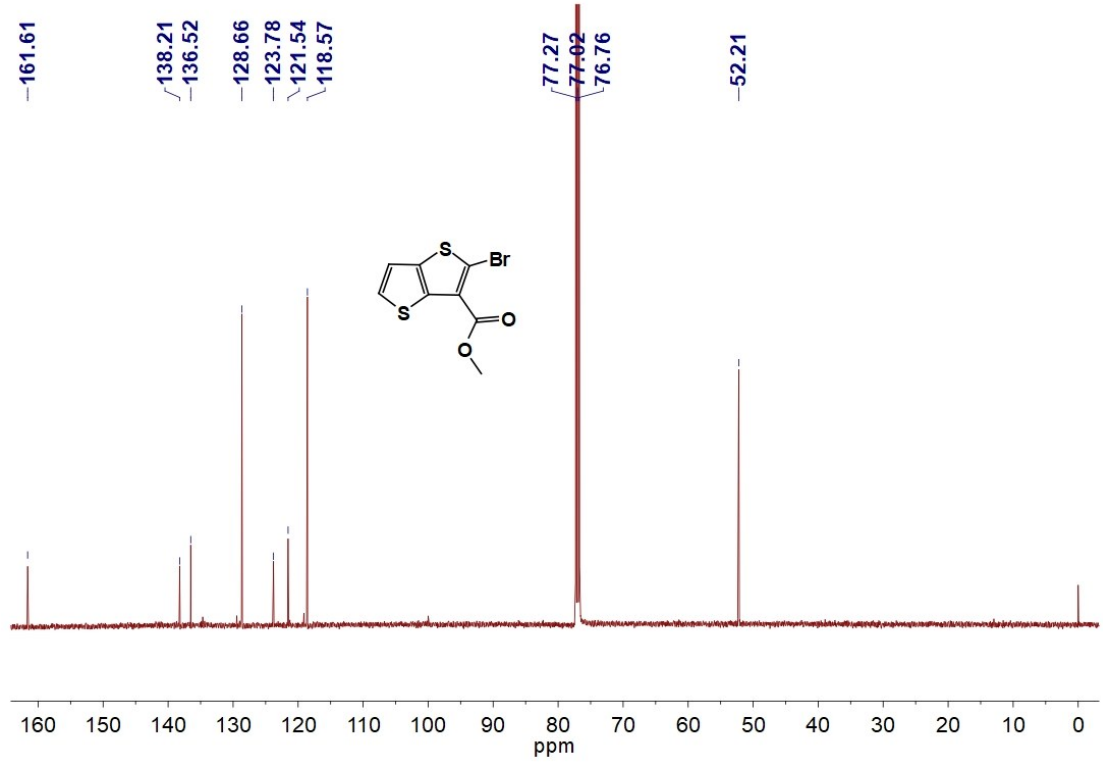

Fig. S14. ^{13}C NMR of compound **4**.

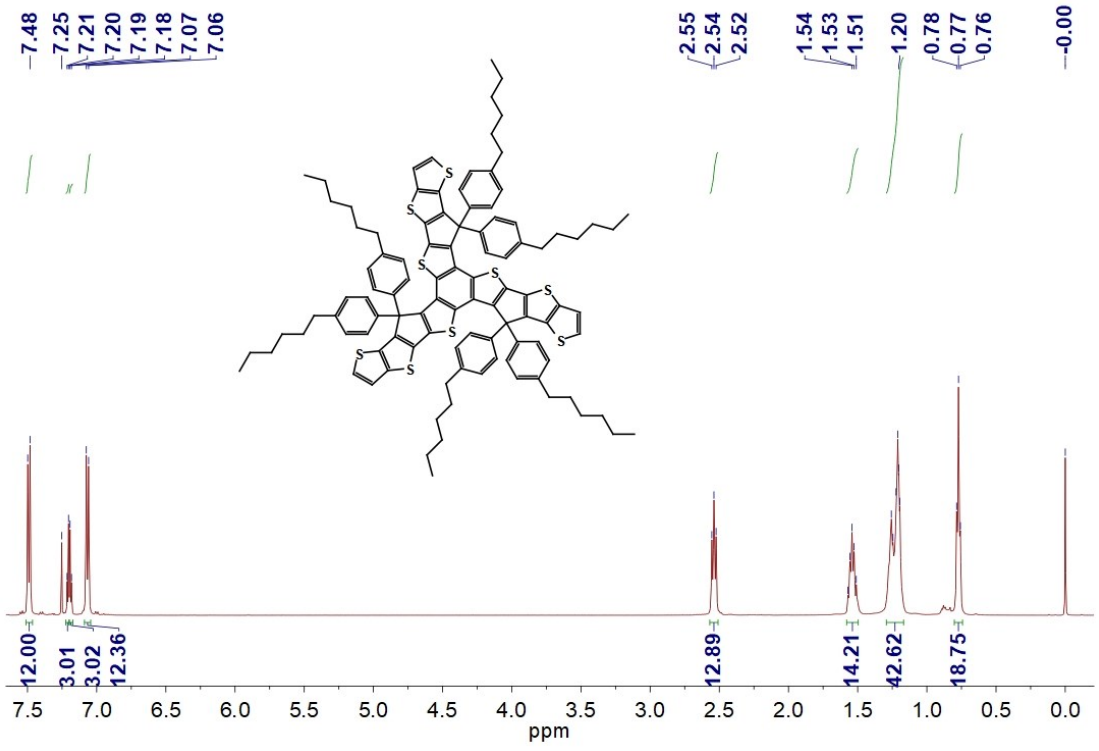

Fig. S15. ^{1}H NMR of **BTTCTT**.

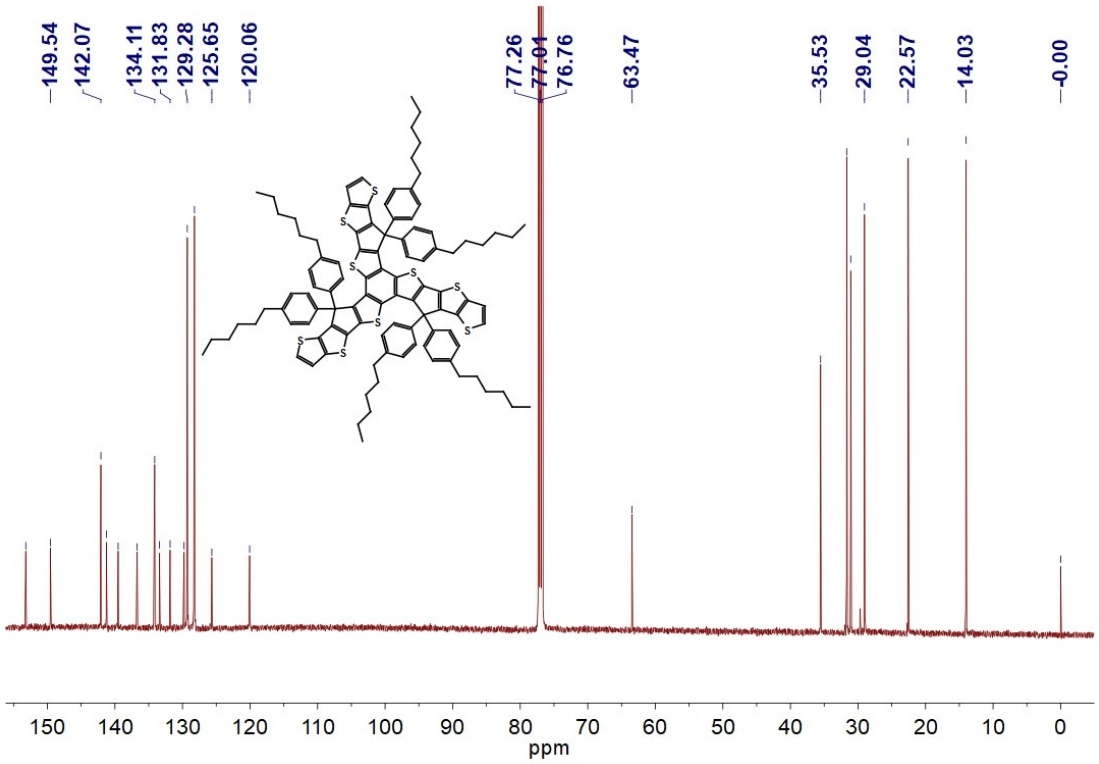

Fig. S16. ^{13}C NMR of **BTTCTT**.

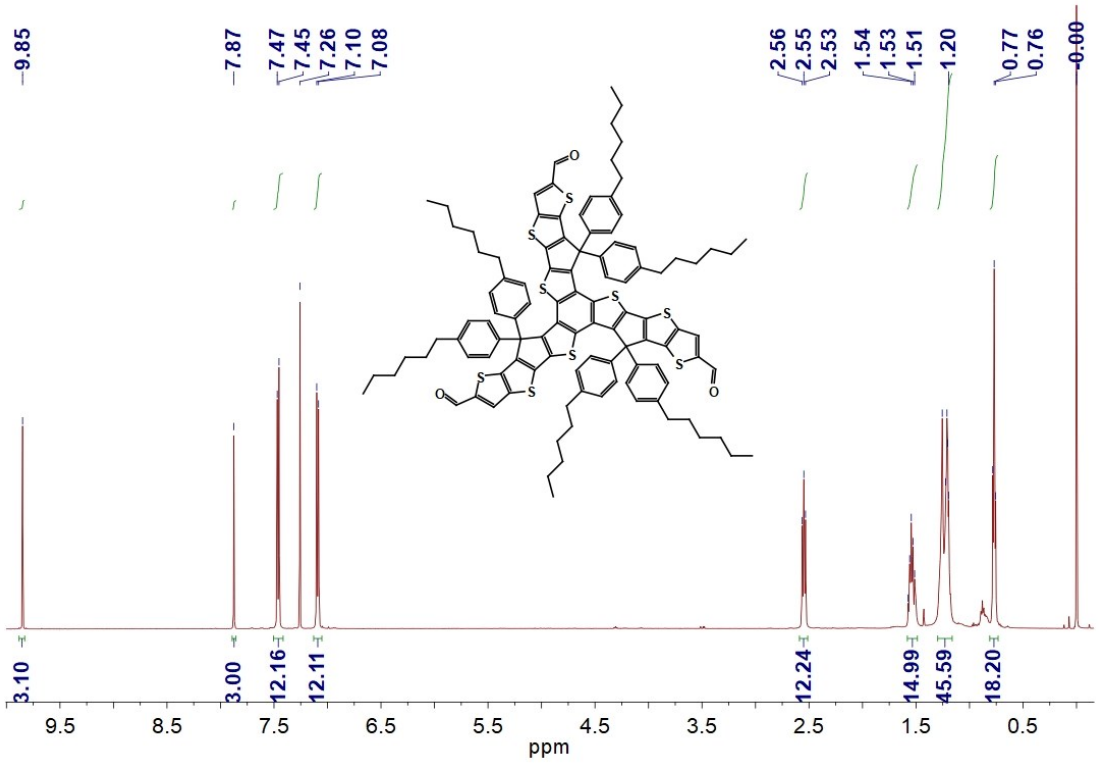

Fig. S17. ^{1}H NMR of **BTTCTT-CHO**.

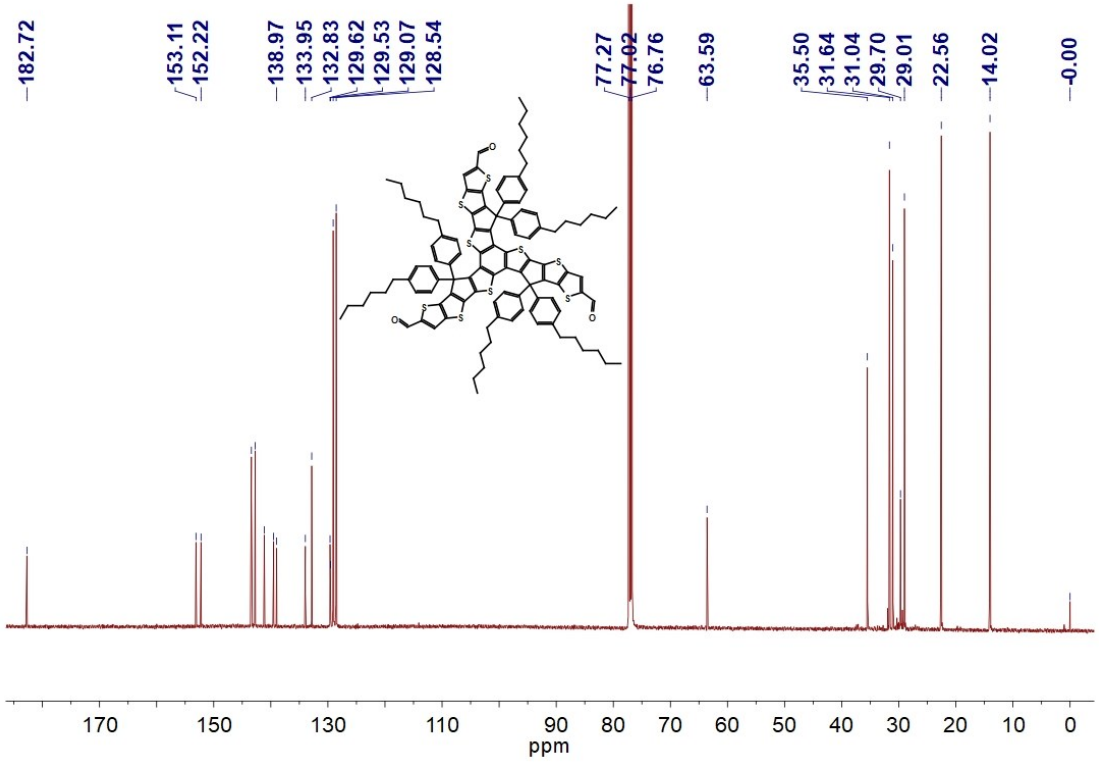

Fig. S18. ^{13}C NMR of **BTTCTT-CHO**.

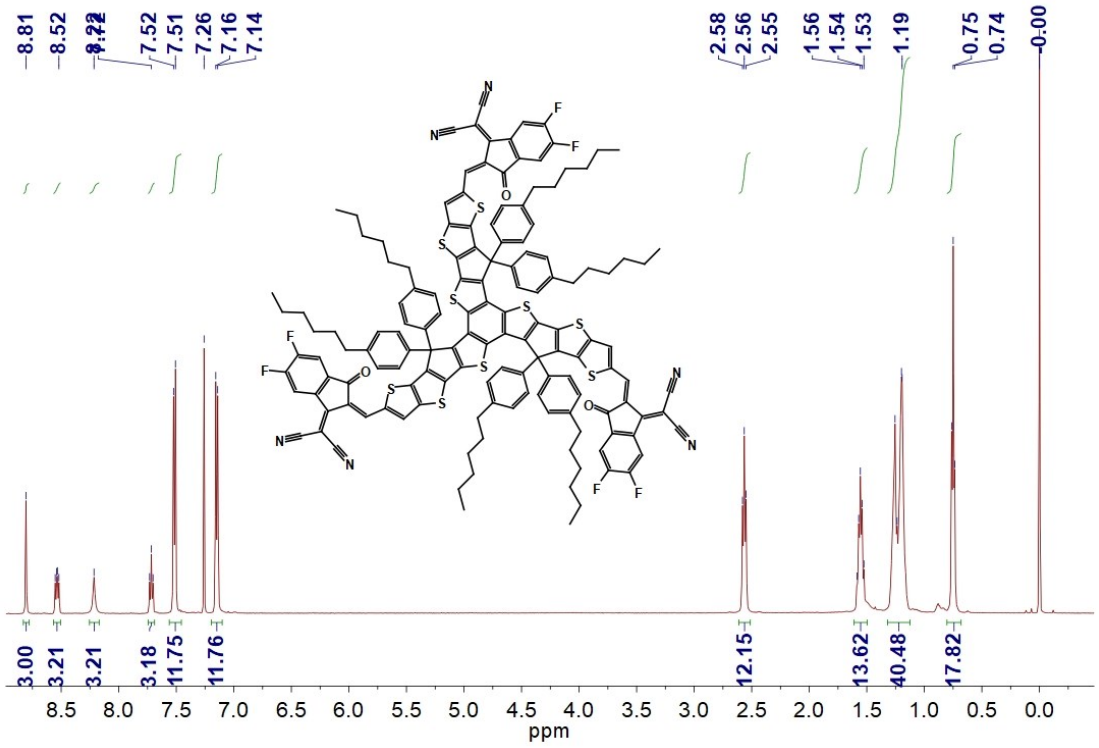

Fig. S19. ^{1}H NMR of **BTTCTT-ICF**.

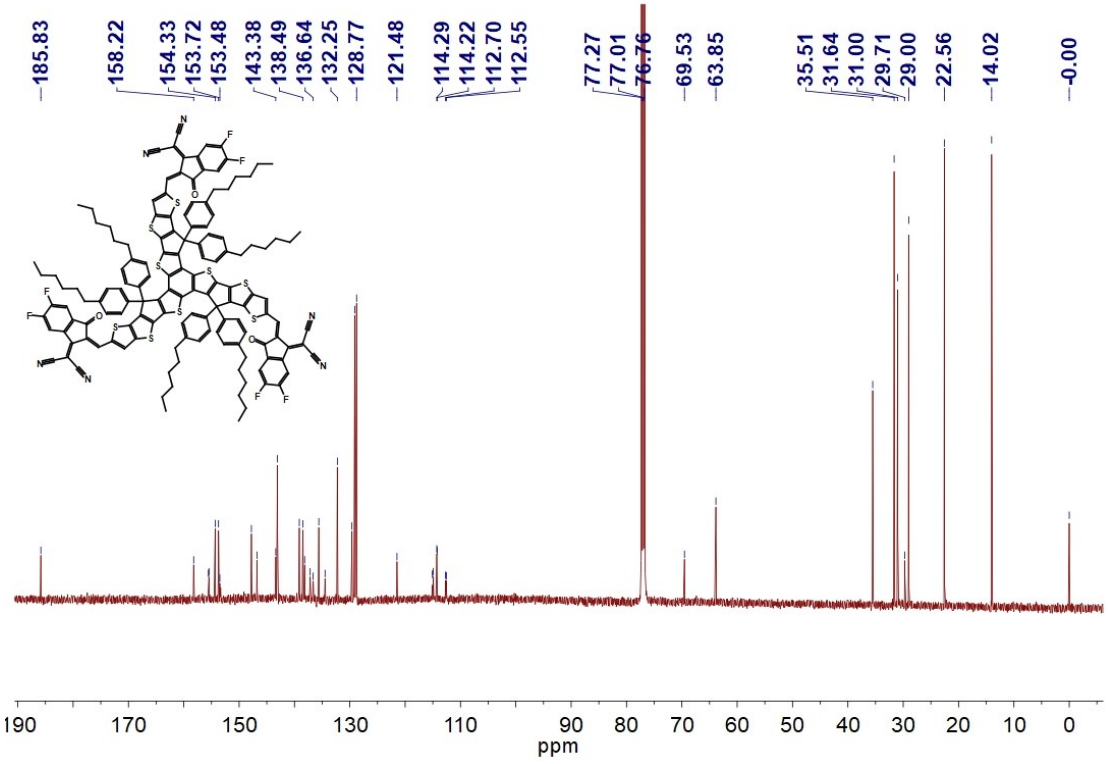

Fig. S20. ^{13}C NMR of **BTTCTT-ICF**.

Table S1. Optical and electrochemical data of **BTTCTT-ICF**.

Acceptor	UV (λ_{max} [nm])		ε_{max}[a] [M^{-1} cm^{-1}]	E_g opt[b] [eV]	HOMO[c] [eV]	LUMO[c] [eV]	E_g ec[d] [eV]
	Solution	Film					
BTTCTT-ICF	683	711	3.6×10^5	1.54	-5.64	-4.08	1.56

[a.] Molar extinction coefficient at λ_{max} in solution.
[b.] Optical bandgaps calculated from the absorption edge of thin film.
[c.] HOMO/LUMO energy level estimated from the onset of oxidation potential and reduction potential by CV measurement, respectively.
[d.] Electrochemical bandgaps calculated from HOMO/LUMO energy levels.

Table S2. The photovoltaic performance of the devices based on **PM6**: **BTTCTT-ICF** with different solvent (D/A = 1:1).

Solvent	V_{oc} [V]	J_{sc} [mA cm^{-2}]	FF [%]	PCE [%]
o-DCB	0.88	11.58	44.08	4.49
CB	0.8	14.45	47.65	5.51
CF	**0.91**	**15.75**	**45.06**	**6.46**

Table S3. The photovoltaic performance of the devices based on **PM6**: **BTTCTT-ICF** with different donor/acceptor (D/A) ratio (The solvent is CF).

D/A	V_{oc} [V]	J_{sc} [mA cm^{-2}]	FF [%]	PCE [%]
1:1	0.91	15.75	45.06	6.46
1:1.2	0.91	15.99	48.59	7.07
1:1.5	**0.92**	**14.89**	**52.30**	**7.16**
1:1.8	0.91	14.37	50.66	6.63

Table S4. The photovoltaic performance of the devices based on **PM6**: **BTTCTT-ICF** at different thermal annealing temperature (The solvent is CF, D/A = 1:1.5).

Thermal annealing temperature [°C]	V_{oc} [V]	J_{sc} [mA cm^{-2}]	FF [%]	PCE [%]
--	0.92	14.89	52.30	7.16
80	0.92	15.05	54.30	7.52
120	0.91	15.08	54.81	7.52
160	0.91	14.45	58.72	7.73
200	**0.89**	**15.41**	**58.64**	**7.98**
240	0.85	14.30	51.45	6.25

Table S5. The photovoltaic performance of the devices based on **PM6**: **BTTCTT-ICF** with different device structures.

Active layer	V_{oc} [V]	J_{sc} [mA cm^{-2}]	FF [%]	PCE [%]
as-cast [a]	0.92	14.89	52.30	7.16
thermal annealing [a, c]	0.89	15.41	58.64	7.98
as-cast [b]	0.93	15.65	63.53	9.25
thermal annealing [b, c]	0.91	16.77	68.08	10.39

[a.] Conventional device structure: ITO/PEDOT: PSS/active layer/PDINO/Al.
[b.] Inverted device structure: ITO/ZnO/active layer/MoO_3/Ag.
[c.] Thermal annealing at 200 °C for 10 min.

Table S6. The photovoltaic performance of the devices based on **PM6**: **BTTCTT-ICF** with different additive contents in inverted structures (The solvent is CF, D/A = 1:1.5, 200 °C thermal annealing).

Additive contents	V_{oc} [V]	J_{sc} [mA cm^{-2}]	FF [%]	PCE [%]
none	**0.91**	**16.77**	**68.08**	**10.39**
0.1% DIO	0.91	16.53	68.04	10.23
0.3% DIO	0.9	16.35	68.25	10.04
0.5% DIO	0.87	16.75	67.82	9.88
0.1% CN	0.9	16.55	69.57	10.36
0.3% CN	0.89	16.80	66.30	9.91
0.5% CN	0.9	16.34	66.44	9.77

Table S7. Summarized photovoltaic performance of the devices based on star-shaped FREAs.

Acceptor	Donor	V_{oc} [V]	J_{sc} [mA cm^{-2}]	FF [%]	PCE [%]	Ref.
Tr(Hex)$_6$-3BR	PTB7-Th	1.02	5.92	33.4	2.10	1
Para-TrBRCN	PTB7-Th	0.95	13.75	63.5	8.29	2
Meta-TrBRCN	PTB7-Th	0.94	16.75	64.5	10.15	2
TrBTIC	P3HT	0.88	13.04	71.9	8.25	3
TITT-3IC	PTB7-Th	0.80	10.32	46.86	3.87	4
TITT-3ICF	PTB7-Th	0.68	12.64	49.62	4.26	4
BTCDT-IC	J61	0.92	9.75	59.0	5.30	5
BTCDT-ICF	J61	0.73	16.93	65.6	8.11	5
FBTIC	**PM6**	0.947	14.1	75.4	10.1	6
TF1	PBDB-T	0.91	15.9	69	10	7
TF2	PBDB-T	0.90	15.4	68	9.4	7
BTTCTT-ICF	**PM6**	0.91	16.77	68.08	10.39	This work

Table S8. The photovoltaic performance of the devices based on **PM6**: **BTTCTT-ICF** after thermal annealing at 200 °C for different time.

Thermal annealing time [min]	V_{oc} [V]	J_{sc} [mA cm^{-2}]	FF [%]	PCE [%]
10	0.91	16.77	68.08	10.39
20	0.9	16.98	65.71	10.04
30	0.89	17.13	64.87	9.89
45	0.88	17.07	62.84	9.44
60	0.87	17.52	60.97	9.29
120	0.86	17.96	58.61	9.05
180	0.86	17.86	58.44	8.98
360	0.85	17.53	54.38	8.10
720	0.85	17.73	53.30	8.03

Table S9. The hole mobility (μ_h) and electron mobility (μ_e) of **PM6**: **BTTCTT-ICF** as-cast and thermal annealed blend films.

	μ_e [cm^2 V^{-1} s^{-1}]	μ_h [cm^2 V^{-1} s^{-1}]	μ_h/μ_e
as-cast	3.57×10^{-6}	1.90×10^{-4}	53.2
thermal annealing	1.59×10^{-5}	2.80×10^{-4}	17.6

References:

1. K. Lin, B. Xie, Z. Wang, R. Xie, Y. Huang, C. Duan, F. Huang and Y. Cao, Star-shaped electron acceptors containing a truxene core for non-fullerene solar cells, *Org. Electron.*, 2018, **52**, 42-50.

2. W. Wu, G. Zhang, X. Xu, S. Wang, Y. Li and Q. Peng, Wide bandgap molecular acceptors with a truxene core for efficient nonfullerene polymer solar cells: linkage position on molecular configuration and photovoltaic properties, *Adv. Funct. Mater.*, 2018, **28**, 1707493.

3. X. Xu, G. Zhang, L. Yu, R. Li and Q. Peng, P3HT-based polymer solar cells with 8.25% efficiency enabled by a matched molecular acceptor and smart green-solvent processing technology, *Adv. Mater.*, 2019, **31**, e1906045.

4. W. Wang, X. Wu, H. Hang, H. Li, Y. Chen, Q. Xu, H. Tong and L. Wang, Star-shaped and fused electron acceptors based on C_{3h}-symmetric coplanar trindeno[1,2-b:4,5-b':7,8-b'']trithiophene core for non-fullerene solar cells, *Chem. Eur. J.*, 2019, **25**, 1055-1063.

5. X. Wu, W. Wang, H. Hang, H. Li, Y. Chen, Q. Xu, H. Tong and L. Wang, Star-shaped fused-ring electron acceptors with a C_{3h}-symmetric and electron-rich benzotri(cyclopentadithiophene) core for efficient nonfullerene organic solar cells, *ACS Appl. Mater. Interfaces*, 2019, **11**, 28115-28124.

6. G. Cai, W. Wang, J. Zhou, Y. Xiao, K. Liu, Z. Xie, X. Lu, J. Lian, P. Zeng, Y. Wang and X. Zhan, Comparison of linear- and star-shaped fused-ring electron acceptors, *ACS Mater. Lett.*, 2019, **1**, 367-374.

7. Z. Yao, X. Liao, Y. Guo, H. Zhao, Y. Guo, F. Zhang, L. Zhang, Z. Zhu, L. Kloo, W. Ma, Y. Chen and L. Sun, Exploring overall photoelectric applications by organic materials

containing symmetric donor isomers, *Chem. Mater.*, 2019, **31**, 8810-8819.